GEOPHYSICS, VOL. 54, NO. 4 (APRIL 1989); P. 497 507, 11 FIGS.

Discrete linear transformations of potential field data

Jorge W. D. Leão* and João B. C. Silva*

ABSTRACT

We present a new approach to perform any linear transformation of gridded potential field data using the equivalent-layer principle. It is particularly efficient for processing areas with a large amount of data. An $N \times N$ data window is inverted using an $M \times M$ equivalent layer, with M greater than N so that the equivalent sources extend beyond the data window. Only the transformed field at the center of the data window is computed by premultiplying the equivalent source matrix by the row of the Green's matrix (associated with the desired transformation) corresponding to the center of the data window. Since the inversion and the multiplication by the Green's matrix are independent of the data, they are performed beforehand and just once for given values of N, M, and the depth of the equivalent layer. As a result, a grid operator for the desired transformation is obtained which is applied to the data by a procedure similar to discrete convolution.

The application of this procedure in reducing synthetic anomalies to the pole and computing magnetization intensity maps shows that grid operators with $N = 7$ and $M = 15$ are sufficient to process large areas containing several interfering sources. The use of a damping factor allows the computation of meaningful maps even for unstable transformations in the presence of noise. Also, an equivalent layer larger than the data window takes into account part of the interfering sources so that a smaller damping factor is employed as compared with other damped inversion methods.

Transformations of real data from Xingú River Basin and Amazon Basin, Brazil, demonstrate the contribution of this procedure for improvement of a preliminary geologic interpretation with minimum a priori information.

INTRODUCTION

A potential field anomaly is the sum of the gravity or magnetic effects produced by spatial variations of density or magnetic polarization, respectively. As a result, the design of operations which attenuate the unwanted components of the observed anomalies has been of great interest. The first operators designed to process practical data were the second vertical derivative and analytical continuation (Peters, 1949; Henderson and Zietz, 1949; Elkins, 1951; Rosenbach, 1953; Henderson, 1960). Due to limited computing facilities, processors of gravity and magnetic data took advantage of the radial structure of these operators to design radial weights. When convolved with the observed data, the radial weights caused a substantial reduction in the calculations.

Bhattacharyya (1965) obtained analytic continuation and vertical derivatives of the total magnetic field by expanding the total field in a double Fourier series and recomputing the series either at different levels in the case of analytic continuation or using modified series coefficients in the case of derivatives. He also extended the analysis to include the reduction-to-the-pole transformation.

Fuller (1967) pointed out the practical need to design square grid operators and compared the frequency responses of published discrete radial second derivative and analytic continuation operators with the frequency responses of the corresponding theoretical discrete operators. Fuller also noted the convenience of treating the operators as numerical filters whose frequency responses are multiplied by the Fourier spectrum of the observed data in order to produce a filtered spectrum. This alternative to the convolution of the observations with linear operators became particularly important with the advent of the fast Fourier transform (FFT) algorithm (Black and Scollar, 1969; Kanasewich and Agarwal, 1970; Tsay, 1975).

The problem with filtering the data in the frequency domain lies in the imperfections introduced in the data spectrum by aliasing and Gibbs' phenomenon, which are caused by the discretization and truncation of the anomalies, respectively. If the filter operator in the frequency domain is stable, such as filters for upward continuation, integration, and reduction-to-the-pole at high magnetic latitudes, the amplitudes of the imperfections in the data spectrum are either preserved or attenuated. On the other hand, unstable filters, such as those for downward continuation, second vertical derivative, and reduction-to-the-pole at low magnetic latitudes, enhance

Manuscript received by the Editor January 26, 1988; revised manuscript received August 24, 1988.
*Federal University of Para, Brazil, CG-UFPa-Caixa Postal 1611, 66000 Belem, Para, Brazil.

tremendously the amplitude of the spectrum imperfections so that any direct application of such filters produces completely meaningless results. The presence of either random or geologic noise in the data aggravates the problem. The traditional remedy has been either to reduce the noise content in the data (Roy, 1966; Pearson and Skinner, 1982) or to lessen the Gibbs' phenomenon either by computing the discrete Fourier spectrum on a gridding area larger than the area of interest (Tsay, 1975) or by multiplying the data by a suitable window (Paine, 1986). Both procedures, however, present difficulties. The first one can only be partially accomplished because of spectral overlap of the signal and noise. The second procedure may require increased computer time and memory to process large areas, particularly when the filter is unstable as in the case of the reduction-to-the-pole at low magnetic latitudes.

Gunn (1975) presented a unified approach in the wavenumber domain to all linear transformations of interest in potential field data, including linear inversion.

A different approach to linear transformations of potential field data consists in fitting equivalent sources to the observations and recomputing the field due to the equivalent sources using the Green's function corresponding to the desired transformation (Bott and Ingles, 1972; Emilia, 1973). The equivalent-layer technique has been extensively employed in processing satellite magnetic data (Mayhew, 1979; Mayhew et al., 1980; von Frese et al., 1982; Ridgway and Hinze, 1986); it is superior to FFT filtered maps in producing stable reduction-to-the-pole maps at low latitudes (Silva, 1986). One restriction to the application of this technique (and to a lesser extent also of the FFT filtering procedure) has been the huge amount of computer time and memory involved, since, in all applications known by the authors, the computation of the equivalent sources is formulated either as an exactly determined problem or as an overdetermined least-squares problem. As a result, the number of entries in the matrix to be inverted increases with the square of the total number of the observations. A modest 30 × 30 area, for example, requires the inversion of a 900 × 900 matrix. Attempts to divide a large area into small subareas and process them individually incur undesirable edge effects, despite the adoption of some strategies such as overlapping adjacent subareas. Langel et al. (1984) reported a procedure which produces a smooth transition between two adjacent subareas. Unfortunately, no synthetic example is given so that the distortion produced by this procedure cannot be assessed. von Frese et al. (1988) presented an iterative procedure to process large-scale equivalent-source inversions. A small equivalent layer is computed using all observations. The residuals between the observations and the field produced by the equivalent layer are used to calculate another small equivalent layer located at a different place. Further iterations use the residuals between the observations and the field produced by all previously computed equivalent layers.

Here we present a method to perform any linear transformation of potential field data, a method particularly suited to process areas with large amounts of data. An equivalent layer which reproduces exactly the observations is computed by the underdetermined least-squares method using a small data window (typically 7 × 7 points). Next, the transformed field at the center of the data window is obtained by recomputing the field due to the equivalent layer using the appropriate discrete Green's function. Since both the Green's function and the underdetermined least-squares pseudoinverse operators are independent of the observations, these two operators are combined in a single operator having the dimensions of the data window. Since the data are assumed to be regularly spaced, this operator can be applied to the observations by a procedure similar to discrete convolution.

LINEAR TRANSFORMATIONS USING THE EQUIVALENT-LAYER PRINCIPLE

The equivalent-layer principle

By the equivalent-layer principle, a gravity or magnetic anomaly due to arbitrary sources can be reproduced exactly by a continuous, infinite, two-dimensional (2-D) distribution of density or magnetization, respectively. Mathematically, we have

$$t(x, y, z) = K \int_{-\infty}^{\infty} \int_{-\infty}^{\infty} G(x, y, z, x', y') p(x', y', d)\, dx'\, dy', \qquad (1)$$

where K is either the gravitational constant or the magnetic permeability of free space, p is a density or magnetization surface distribution situated at a constant depth d, and G is the Green's function given by

$$G(x, y, z, x', y') = \frac{\partial}{\partial z} [(x - x')^2 + (y - y')^2 + (z - d)^2]^{-1/2} \qquad (2)$$

for the vertical gravity field and

$$G(x, y, z, x', y') = \left[L \frac{\partial}{\partial x} + M \frac{\partial}{\partial y} + N \frac{\partial}{\partial z} \right] \left[\ell \frac{\partial}{\partial x} + m \frac{\partial}{\partial y} + n \frac{\partial}{\partial z} \right] \times [(x - x')^2 + (y - y')^2 + (z - d)^2]^{-1/2} \qquad (3)$$

for the total magnetic field anomaly, where L, M, N and ℓ, m, n are the direction cosines of the geomagnetic field and the total magnetization, respectively, assumed constant in direction.

The discrete, finite equivalent layer

To obtain the surface distribution p, one must solve the integral equation of the first kind given by equation (1). In order to be of any practical use, the distribution p must be discrete and of finite dimensions so that the solution of equation (1) by quadrature is convenient. Following a procedure similar to the one adopted by Silva and Hohmann (1984), the integral equation (1) is transformed into the matrix equation

$$\mathbf{t}^0 = \underline{\mathbf{A}}\mathbf{p}, \qquad (4)$$

where $\mathbf{t}^0$ is a vector of length N containing the observations, $\mathbf{p}$ is a vector of length M of unknown surface densities or magnetizations, and $\underline{\mathbf{A}}$ is the $N \times M$ matrix whose element a_{ij} is the discrete Green's function.

The solution of equation (4) is given by

$$\hat{\mathbf{p}} = \underline{\mathbf{A}}^+ \mathbf{t}^0, \qquad (5)$$

where $\underline{\mathbf{A}}^+$ is either a pseudoinverse (Rao and Mitra, 1971) or a damped approximate inverse (Jupp and Vozoff, 1975) of $\underline{\mathbf{A}}$.

Below we refer to $\underline{\mathbf{A}}^+$ as a D-pseudoinverse. A unique solution of equation (4) is possible only if N is equal to M and if the matrix $\underline{\mathbf{A}}$ is of full rank. Then, $\underline{\mathbf{A}}^+ = \underline{\mathbf{A}}^{-1}$, the true inverse of $\underline{\mathbf{A}}$. The matrix $\underline{\mathbf{A}}$ is usually ill-conditioned so that estimates of $\mathbf{p}$ using $\underline{\mathbf{A}}^{-1}$ are extremely unstable in the presence of random noise and interference produced by sources located beyond the limits of the finite equivalent layer. In order to overcome this difficulty, D-pseudoinverses other than the true inverse must be used, pseudoinverses which have the property of producing stable solutions of equation (4). Depending on the particular choice of the D-pseudoinverse, there may be several estimators $\hat{\mathbf{p}}$.

Once a particular estimator is selected, a desired linear transformation of the original field $\mathbf{t}$ is obtained by

$$\mathbf{t} = \underline{\mathbf{B}}\hat{\mathbf{p}}, \tag{6}$$

where $\underline{\mathbf{B}}$ is the Green's function associated with the desired linear transformation. Combining equations (5) and (6), we have

$$\mathbf{t} = \underline{\mathbf{B}}\underline{\mathbf{A}}^+\mathbf{t}^0. \tag{7}$$

Evidently, the transformation is not unique but will depend on the particular choice of $\underline{\mathbf{A}}^+$.

The standard solutions

Two D-pseudoinverses have been commonly employed: the generalized inverse (Penrose, 1955) obtained from the singular value decomposition of a matrix (e.g., von Frese et al., 1981 and Langel et al., 1984) and the ridge regression inverse (Hoerl and Kennard, 1970a, b) (e.g., Silva, 1986).

The use of either the generalized inverse or ridge regression as D-pseudoinverses produces stable estimates, even in the presence of interfering sources (Silva and Hohmann, 1984). This stability represents an advantage over FFT filtering in the case of unstable linear transformations.

In all of the above examples, the determination of the equivalent-layer estimate is formulated either as an exactly determined ($N = M$) problem or an overdetermined ($N > M$) least-squares problem. In both cases, the limited number of point sources in the equivalent layer ($M \leq N$) implies the use of a limited layer which cannot, therefore, account satisfactorily for the effects of sources lying outside its limits. These effects can be accounted for only by assigning either a low rank in the generalized inverse approach or a large damping factor in the ridge regression approach, introducing in either case a substantial bias in the solution. Also, computer time and storage limitations in the computation of the D-pseudoinverse operators prevent their application to areas containing more than about a hundred observations.

Proposed method

The method we present in this paper can be applied to regularly spaced data only, so we assume that the measured observations were interpolated in a rectangular grid by a suitable gridding algorithm.

The proposed method is characterized by two distinctive features. The first is the choice of the underdetermined least-squares D-pseudoinverse to compute the equivalent layer, and the second is the combination of the D-pseudoinverse with the discrete Green's function corresponding to the desired transformation. This combination leads to a great simplification of the operations and an improvement in the performance of the method over previous approaches.

The D-pseudoinverse employed in the method is given by

$$\underline{\mathbf{A}}^+ = \underline{\mathbf{A}}^T(\underline{\mathbf{A}}\underline{\mathbf{A}}^T)^{-1}. \tag{8}$$

The matrix $\underline{\mathbf{A}}\underline{\mathbf{A}}^T$ is usually ill-conditioned, so that the inversion is unstable in the presence of noise. One procedure to deal with this problem consists of adding a small positive number λ to each diagonal element of the normalized matrix $\underline{\mathbf{A}}\underline{\mathbf{A}}^T$. Equation (8) is then modified to

$$\underline{\mathbf{A}}^+ = \underline{\mathbf{A}}^T\underline{\mathbf{D}}(\underline{\mathbf{D}}\underline{\mathbf{A}}\underline{\mathbf{A}}^T\underline{\mathbf{D}} + \lambda\underline{\mathbf{I}})^{-1}\underline{\mathbf{D}}, \tag{9}$$

where $\underline{\mathbf{D}}$ is the normalizing diagonal matrix with elements

$$d_{ii} = \left[\sum_{j=1}^{M} a_{ij}^2\right]^{-1/2}, \qquad i = 1, \ldots, N. \tag{10}$$

The use of the D-pseudoinverse defined in equation (8) has the advantage that an increase in the number M of discrete equivalent point sources does not increase appreciably either the memory or the processing time required to obtain the D-pseudoinverse, because the matrix to be inverted is $N \times N$ instead of $M \times M$. Therefore, the discrete equivalent layer may be conveniently extended beyond the data window limits in order to take the interfering sources into account. However, in order to make the matrix inversion feasible, a small data window must be employed, so that an area containing a large number of observations must be processed by parts. In this case, the transformation operator $\underline{\mathbf{B}}\underline{\mathbf{A}}^+$ in equation (7) is applied to adjacent data windows, and prominent discontinuities appear at the borders of the windows. In order to minimize these edge effects, we compute the transformed field only at the central point of each data window. This is equivalent to modifying equation (7) by premultiplying $\underline{\mathbf{A}}^+$ by the central row of the discrete Green's function matrix $\underline{\mathbf{B}}$, yielding

$$t_i = \mathbf{b}_i^T\underline{\mathbf{A}}^+\mathbf{t}^0, \tag{11}$$

where $\mathbf{b}_i^T$ is the central row of matrix $\underline{\mathbf{B}}$ and t_i is the transformed field at the central point of the data window. Substituting equation (9) into equation (11), we have

$$t_i = \mathbf{c}_i^T\mathbf{t}^0, \tag{12}$$

where

$$\mathbf{c}_i^T = \mathbf{b}_i^T\underline{\mathbf{A}}^T\underline{\mathbf{D}}(\underline{\mathbf{D}}\underline{\mathbf{A}}\underline{\mathbf{A}}^T\underline{\mathbf{D}} + \lambda\underline{\mathbf{I}})^{-1}\underline{\mathbf{D}}. \tag{13}$$

Since the data are assumed to be regularly spaced at a horizontal plane, equation (13) is the same for any data window. As a result, equation (12) is applied to the whole area by an operation similar to discrete convolution. That is, after computing the transformed field at the data window center, the operator $\mathbf{c}_i^T$ is moved one unit along the x axis and the process is repeated until a complete row of transformed values is obtained. The operator then moves one unit along the y axis, and so forth, until the whole area is processed.

The damping factor λ is selected by producing transformed fields for increasing values of λ and choosing the one for which there is no qualitative change in the transformed field with respect to that for the previous value. The sizes of the

discrete equivalent layer and the data window should be the smallest possible in order to reduce CPU requirements. However, they should at the same time be large enough to guarantee that a single source at the border of the equivalent layer has negligible effect at points above the center of the layer and to assure a minimum edge effect at the central point of the data window in the convolution-like operation.

Bott (1967) employed this strategy of computing the processed field only at the center of the data window to obtain equivalent source intensities from one-dimensional (1-D) magnetic data. However, he used the exactly determined D-pseudoinverse; that is, the inverse for which the number of equivalent point sources is equal to the number of points in the data window. In order to extend the finite equivalent layer beyond the data window limits, the discrete equivalent sources (assumed to be thin contiguous vertical prisms) at the borders were taken to have a larger width than the central sources.

As will be demonstrated in next section by a synthetic example, the use of the strategy described above in conjunction with the overdetermined least-squares D-pseudoinverse may not be sufficient to produce good results. Since the number of the point sources in this case is smaller than the number of observations in the data window, it is difficult to extend the finite equivalent layer beyond the data window limits while keeping the distance between the point sources small in order to maintain a reasonable approximation to the continuous equivalent layer by a discrete one. Consequently, the equivalent layer is unable to take into account the sources outside the data window, so that in the overdetermined case a larger value of λ must be employed than in the underdetermined case in order to produce stable solutions.

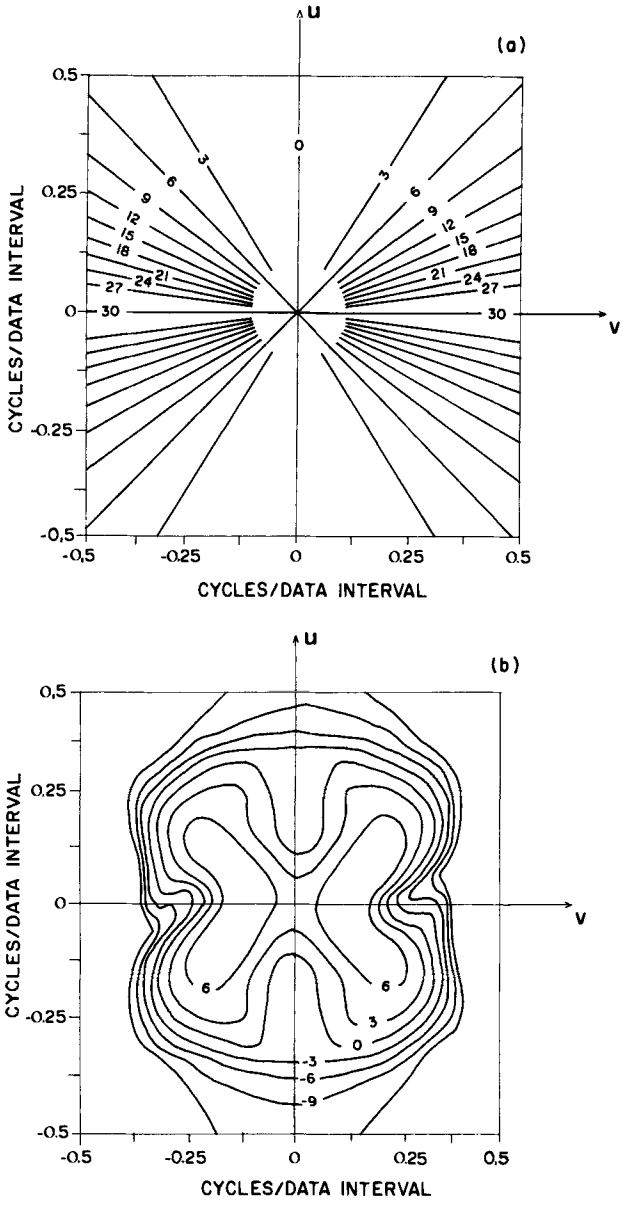

FIG. 1. Frequency response for (a) theoretical and (b) stabilized reduction-to-the-pole filter with $\lambda = 0.1$. The geomagnetic field and magnetization inclinations are 10 degrees and the geomagnetic field and magnetization declinations are 0 degrees. Contour interval is 3 dB.

REDUCTION-TO-THE-POLE AND MAGNETIZATION MAPPING

In this section, we apply the proposed method to synthetic and real anomalies using reduction-to-the-pole at low magnetic latitudes and apparent magnetization mapping transformations as examples. These transformations are both unstable operations and provide good examples of the method's ability to deal with pronounced instability even in the presence of random noise and interfering sources. Also, these transformations are very important in interpreting magnetic data, since they are usually capable of contributing significantly to the geologic knowledge of an area with minimum a priori information.

Analysis of the reduction-to-the-pole operator

As pointed out above, the equivalent-layer approach can produce stable operators to realize unstable transformations of potential field data. The proposed method applies the derived stable operators by means of a procedure similar to convolution in the spatial domain. Therefore, it is instructive to analyze the operator's frequency response and compare that response with the theoretical frequency response of the transformation in question. This was done for the reduction-to-the-pole operator at an inclination of 10 degrees and declination of 0 degrees (Figure 1). Figure 1a displays the amplitude spectrum of the theoretical reduction-to-the-pole filter (Gunn, 1975). The conspicuous enhancement (30 dB) at $\theta = -90$ degrees [$\theta = \arctan(v/u)$], which corresponds to the geomagnetic and magnetization azimuth of 0 degrees with respect to the x axis (geographic north), is the source of instability in reducing magnetic anomalies to the pole at low latitudes. The closer the anomaly is to the equator, the more pronounced is the enhancement. Figure 1b shows the 32×32 discrete amplitude response (calculated by FFT) of the stabilized reduction-to-the-pole operator obtained from equation (13), with $\lambda = 0.1$. Note in Figure 1b that the overall features of the theoretical filter are retained at low wavenumbers, although the maximum amplification is much smaller (9 dB). At high wavenumbers, however, the operator produces attenuation only, regardless of the azimuth. Therefore, use of the parameter λ is analogous to low-pass wavenumber filtering.

Applications to synthetic anomalies

Our method was applied to the synthetic total field anomalies (Figure 2) produced by vertical prisms whose plan views are also displayed. The magnetic field is computed at points of a 31 × 46 grid. The unit employed to express all linear dimensions is the "observation" grid unit. Prisms belonging to group A (A1 through A6) have a magnetization intensity of 1.5 A/m, and the depths to the top and bottom are 2 and 6 units, respectively. Prisms belonging to group B (B1 through B4) have semiinfinite depth extents, tops at a depth of 2 units, and a magnetization intensity of 0.9 A/m. All prisms are magnetized by induction only, and the geomagnetic field has an inclination of 10 degrees and azimuth of 20 degrees to the east relative to the x axis (geographic N-S).

Figure 3 shows the theoretical anomaly at the magnetic pole. Note that the resolution of this map is not sufficient to isolate the sources belonging to group B, due to the small horizontal extents of prisms B1, B2, and B3. On the other hand, the prisms from group A are well delineated, with the exception of prism A3.

When the proposed method is applied to synthetic anomalies, the continuous, infinite equivalent layer is approximated by a discrete layer of 225 (15 × 15) point sources having unit grid spacing and grid points located directly below the observations. The data window consists of 49 (7 × 7) points.

As described above, our method makes use of an operation similar to discrete convolution in the spatial domain. Consequently, edge effects inherent to discrete convolution distort the transformed fields at points of a rectangular grid whose widths measured in the x and y directions are one-half the operator dimensions in the x and y directions, respectively. Since in practice it is difficult to assess the severity of the distortion produced at border points, we believe that it is advisible to eliminate them.

Noise-free data.—The anomalies shown in Figure 2 were reduced to the pole using an equivalent layer of doublets with length of 0.1 grid unit and located at a depth of 2 grid units. The result is shown in Figure 4a. Comparing this map with the theoretical anomaly at the pole (Figure 3), we see that the positions of the highs in both figures coincide for most anomalies, while the amplitudes are slightly attenuated. The amplitude of the anomaly associated with prism A5 in Figure 4a is just half the true amplitude. This is probably due to the strong interference of the adjacent bodies (A1, A2, A4, and A6), showing that the reduced-to-the-pole map does not have sufficient resolution to isolate body A5.

For comparison, in Figure 4b the anomalies of Figure 2 were reduced to the pole using a method similar to the one we propose but employing an overdetermined, instead of underdetermined, least-squares method. In this case the equivalent layer has 25 (5 × 5) points, while the data window consists of 49 (7 × 7) points. As compared with Figure 4a, Figure 4b shows a strong trend along N50W. This trend is introduced by edge effects in the discrete equivalent layer, which is now too small to take the interfering sources into account. The appearance of trends like these might greatly distort the geologic interpretation of the magnetic anomalies.

Figure 5 shows the magnetization intensity map produced by an equivalent layer of monopoles at a depth of 2 units using the reduced-to-the-pole anomaly of Figure 4a as input. A layer of monopoles instead of doublets was selected because it produces greater resolution of the sources, probably due to the fact that the intensities of the positive and negative poles in a layer of monopoles are independent of each other, while in a layer of doublets there must be couples of poles with opposite signs having the same intensity. Figure 5 shows remarkably better resolution than the reduced-to-the-pole map of Figure 4a, particularly for the anomalies associated with prisms from group B. Since the depth of the equivalent layer

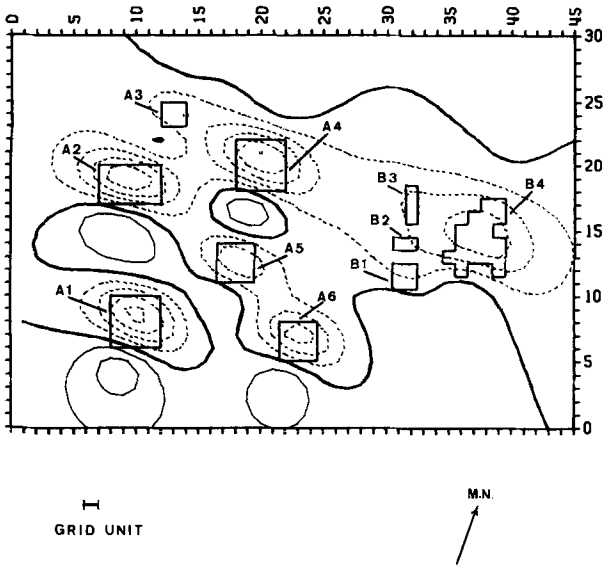

FIG. 2. Total synthetic field produced by indicated vertical prisms. Both the geomagnetic field and magnetization have inclinations of 10 degrees and declinations of 20 degrees. The dashed lines indicate negative contours and the contour interval is 25 nT.

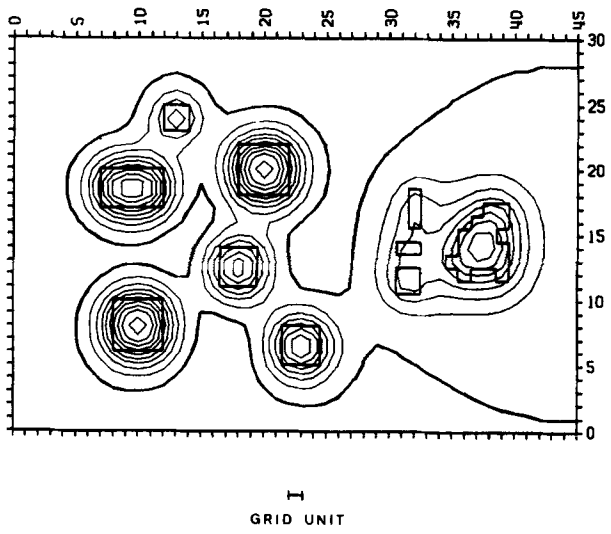

FIG. 3. Total theoretical field at the pole produced by the prisms shown in Figure 2. The thick line represents the zero contour and the thinner lines represent positive values. Contour interval is 25 nT.

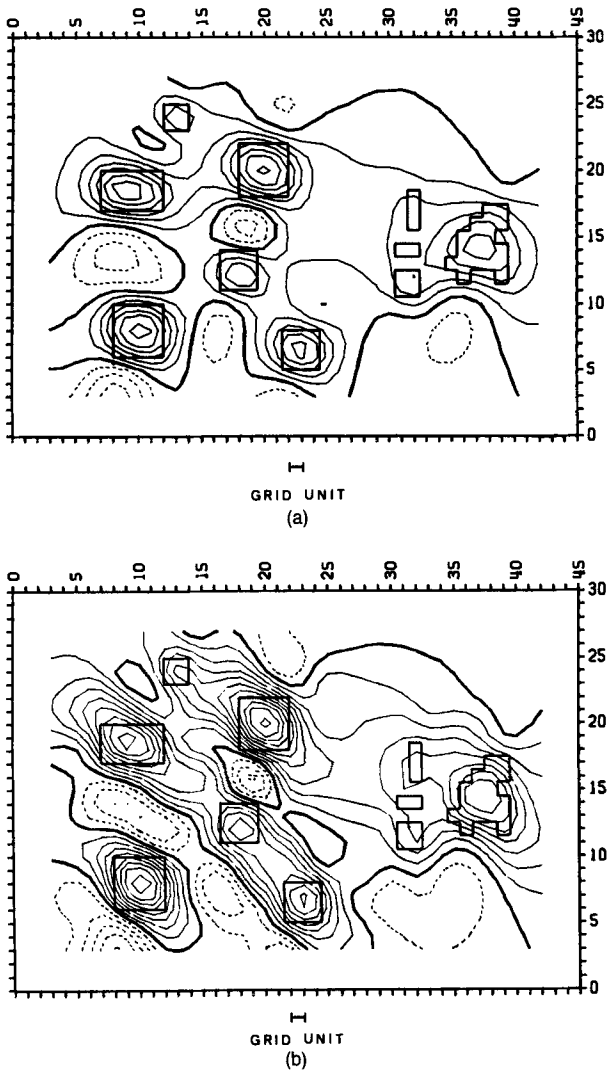

FIG. 4. Total field at the pole obtained by applying our method to the total field shown in Figure 2 with $\lambda = 10^{-5}$ and using (a) underdetermined least-squares and (b) overdetermined least-squares. Dashed lines represent negative values and the contour interval is 25 nT.

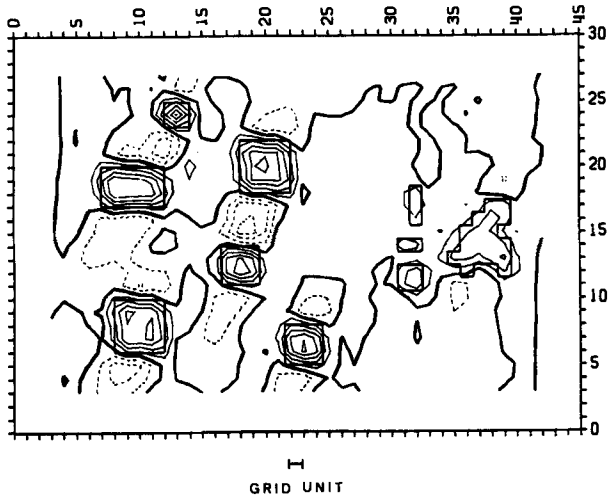

FIG. 5. Magnetization computed from the reduced-to-the-pole map of Figure 4a with $\lambda = 0.005$. Dashed lines represent negative values and the contour interval is 0.25 A/m.

coincides with the top of the sources, the maximum computed magnetization values are close to their true values. The deeper the equivalent layer, the higher the computed magnetization values. This is a consequence of the theoretical ambiguity involving potential field data as demonstrated by the equivalent layer principle. Bodies having horizontal dimensions close to a single grid unit, such as B1, B2, and B3, produce maximum computed magnetization values substantially smaller than the corresponding actual values.

An interesting and consistent feature in all the computed magnetization maps is the delineation of the horizontal section of the sources by the half-maximum contour (Silva and Hohmann, 1984).

Noise-corrupted data.—In order to investigate the effect of Gaussian noise on the reduction-to-the-pole transformation using FFT filtering and our method, the total field anomaly due to the same prisms shown in Figure 2 was recomputed at points of a 32 × 64 grid and Gaussian noise with zero mean and a standard deviation of 5 nT was added. The resulting noise-corrupted map is shown in Figure 6a (only the 31 × 46 grid points of the previous figures are shown).

Figure 6b displays the reduced-to-the-pole anomaly using our method at the same 31 × 46 grid employed in the previous figures. Figure 7 shows the reduced-to-the-pole anomaly obtained by the FFT filtering technique in the wavenumber domain (only the 31 × 46 grid points of the previous figures are shown). A comparison among Figures 6a, 6b, and 7 shows that our method is stable and produces useful reduced-to-the-pole maps even in the presence of random noise and interfering sources, whereas the theoretical filter's instability at low latitudes yields meaningless transformed anomalies. As a result, the filtering method cannot be used directly at low latitudes either to reduce total field anomalies to the pole or to obtain a magnetization map.

Applications to real anomalies

Amazon Basin.—Figure 8a shows the total intensity aeromagnetic map from a survey flown in 1960 over a portion of the middle Amazon Basin, Brazil. The flight lines were oriented in the N-S direction and spaced about 2 km apart. The original data were subsequently interpolated, producing a square grid of points with a spacing of 1 km. The surveyed area covers 277 km in the E-W direction and between 164 and 192 km in the N-S direction, making a total of about 52 000 grid points. The local geomagnetic field in 1960 had inclination of 18 degrees and declination of −6 degrees. A conspicuous feature in Figure 8a is the high noise level caused by several factors, such as instrumentation errors, poor choice of flight line orientation, and interpolation.

The middle Amazon Basin consists of about 3.5 km of sediments deposited between Silurian and Quaternary times over a granite-gneiss basement. The sediments were intruded by dikes and sills of diabase at the end of the Jurassic period (Andrade and Cunha, 1971). There is evidence from gravity data for the presence of huge intracrustal mafic bodies (Linsser, 1974). The observed magnetic anomalies in Figure 8a may be associated either with the Jurassic diabase dikes and sills or with the deeper intrabasement mafics.

The total field map of Figure 8a was reduced to the pole

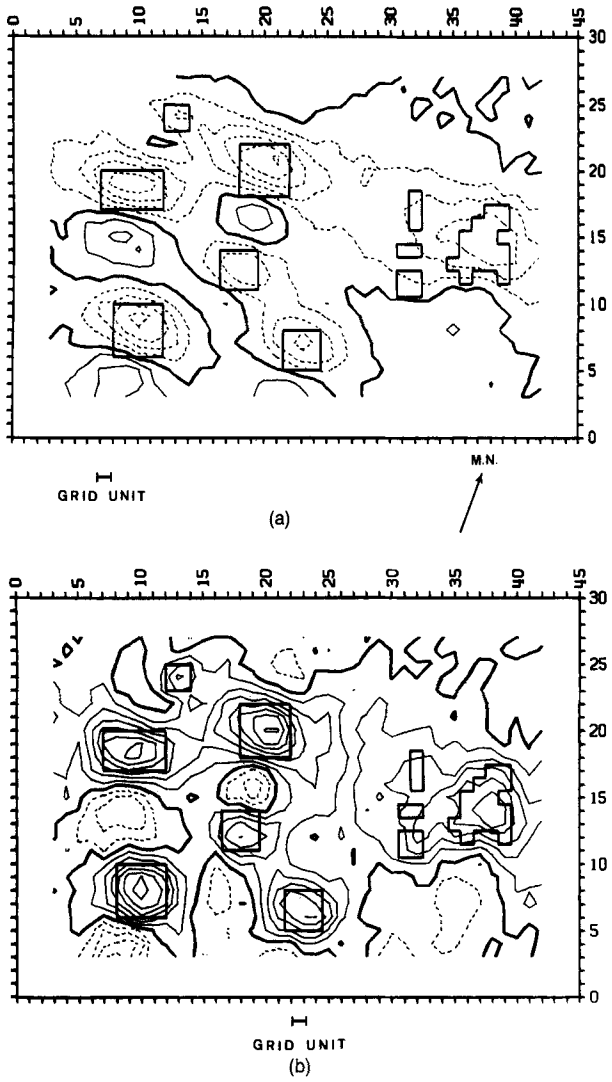

FIG. 6. (a) Total field of Figure 2 corrupted by additive, zero-mean, Gaussian noise with a standard deviation of 5 nT. (b) Total field reduced-to-the-pole by applying our method to the anomaly map shown in Figure 6a with $\lambda = 0.01$. In both figures the dashed lines represent negative values and the contour interval is 25 nT.

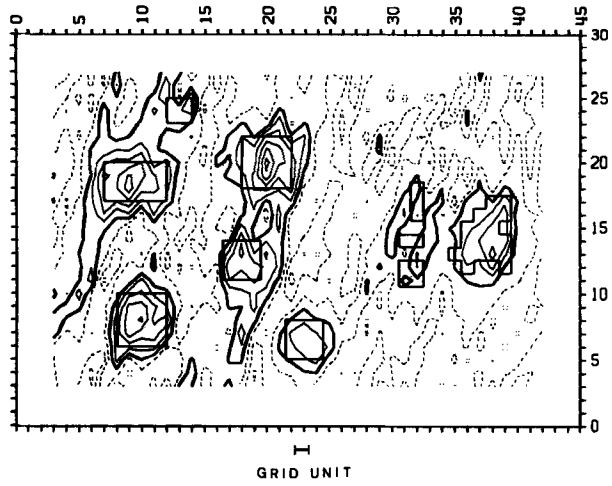

FIG. 7. Total field reduced to the pole obtained by applying the theoretical filter to the anomaly map of Figure 6a, in the wavenumber domain. Dashed lines represent negative values and the contour interval is 50 nT.

using our method, assuming induced magnetization only for the sources. A data window of 7 × 7 points was employed, and a value of $\lambda = 0.5$ was selected to stabilize the transformation. The result is shown in Figure 8b. Except at the southern border and at the northwestern, northeastern, and southeastern corners, the reduced-to-the-pole map consists of positive anomalies, indicating that the assumption of induced magnetization is probably correct. The negative reduced-to-the-pole anomalies in restricted areas suggest a local predominance of remanent magnetization. This hypothesis is supported by a strong positive gravity anomaly coincident with the negative magnetic anomaly at the southeastern corner. This anomaly, and probably most of the other large-scale magnetic anomalies in the area, are presumably caused by the large intrabasement mafic modies. Even though several anomalies in the area are much larger than the 6 km × 6 km window employed (the small hatched area at the northwestern border of Figures 8a and 8b), the method produced a meaningful reduced-to-the-pole map, showing no evidence of edge effects.

Xingú River Basin.—Figure 9 shows the total magnetic field anomaly from a ground survey in the Xingu River Basin. The area is a prospect for copper associated with gold in quartz veins. The data were collected at traverse lines oriented in the N-S direction and spaced 200 m apart. Along each traverse, measurements were made every 50 m. A base level value equal to the average of observations was subtracted from the data. The local geomagnetic field has an inclination of 4.5 degrees and a declination of −16.5 degrees.

The total field anomaly map of Figure 9 displays several high-amplitude anomalies ranging from a few hundred to about a thousand nanoteslas. Note that no useful information besides the association of the anomalies with highly magnetic material can be easily extracted from this figure.

The magnetization map of Figure 10 was obtained by applying our method to the total field anomaly map of Figure 9. A rectangular 400 m × 400 m (9 × 5 points) window was employed, and a value of $\lambda = 0.5$ was selected to stabilize the transformation (first the map of Figure 9 was reduced to the pole assuming induced magnetization only for the sources). Two outstanding features are present in Figure 10. First, there is a sharp isolation of positive and negative anomalies which are highly correlated with mapped itabirite and basic metavolcanic rocks shown in the preliminary geologic map of Figure 11a. Because induced magnetization only was assumed to reduce the magnetic field to the pole, the presence of positive and negative anomalies is interpreted as being produced by rocks with induced and remanent magnetizations, respectively. Second, the spurious E-W trend present in Figure 9, which is caused by an undersampling along the E-W direction, is eliminated, producing a better definition of the anomalies. As a result it was possible, as discussed previously, to delineate the boundary between the two magnetic units (itabirite and metavolcanics) by the half-maximum contour of the magnetization map. The resulting map shown in Figure 11b delineates the two units in the *subsurface* and may represent a substantial contribution to the geologic knowledge of the area. Subsequent drilling at a site mapped in Figure 11b as metavolcanic rock (point D in Figures 11a and 11b) did in fact intersect this type of rock about 40 m below the ground surface, even though in Figure 11a this site had been mapped as schist.

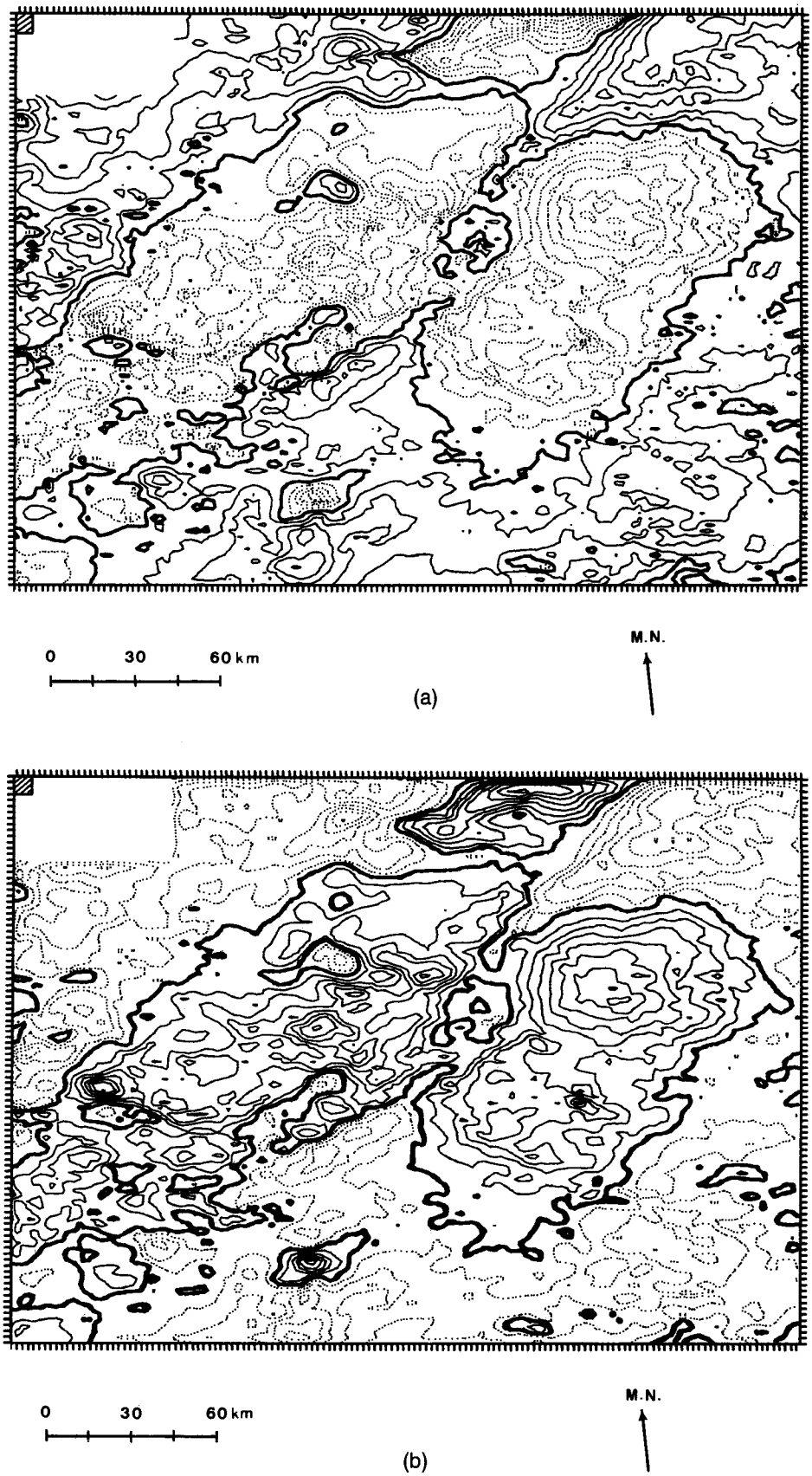

FIG. 8. (a) Total aeromagnetic field map from the Amazon Basin. The geomagnetic field has an inclination of 18 degrees and a declination of −6 degrees. (b) Total field reduced to the pole by applying our method to the anomaly map of Figure 8a with $\lambda = 0.5$. In both figures, the dashed lines represent negative values and the contour interval is 50 nT.

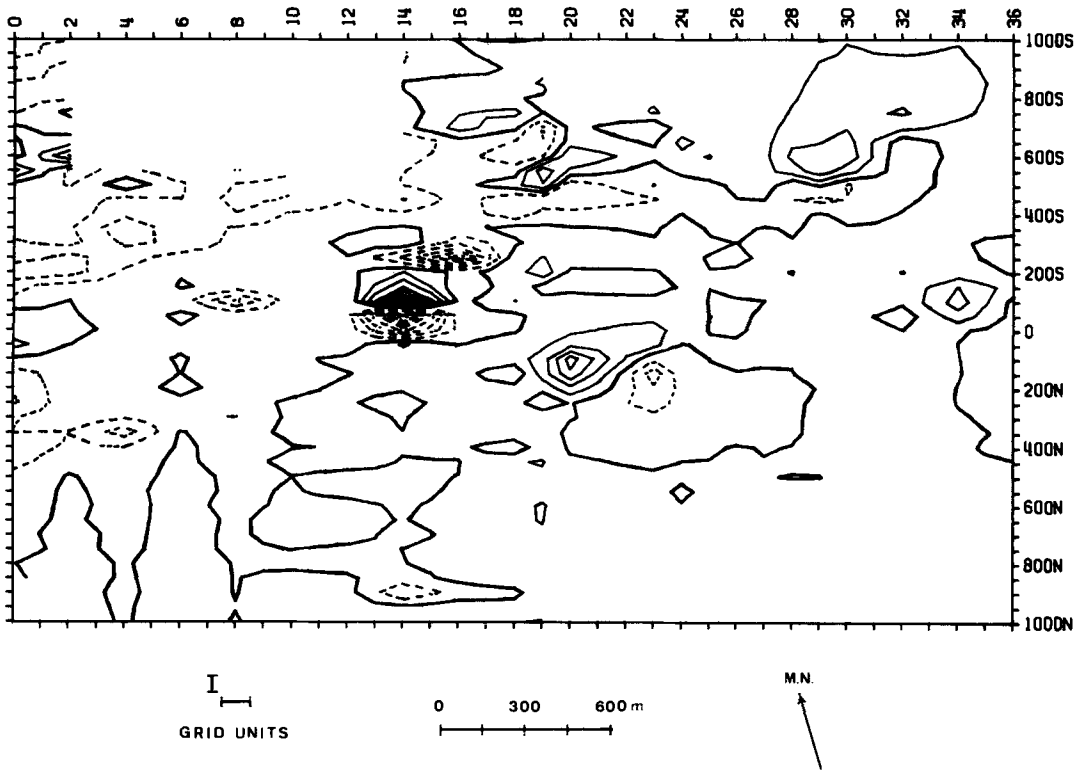

FIG. 9. Total field map of Xingu River Basin area. The geomagnetic field has an inclination of 4.5 degrees and a declination of −16.5 degrees. Dashed lines represent negative values and the contour interval is 100 nT.

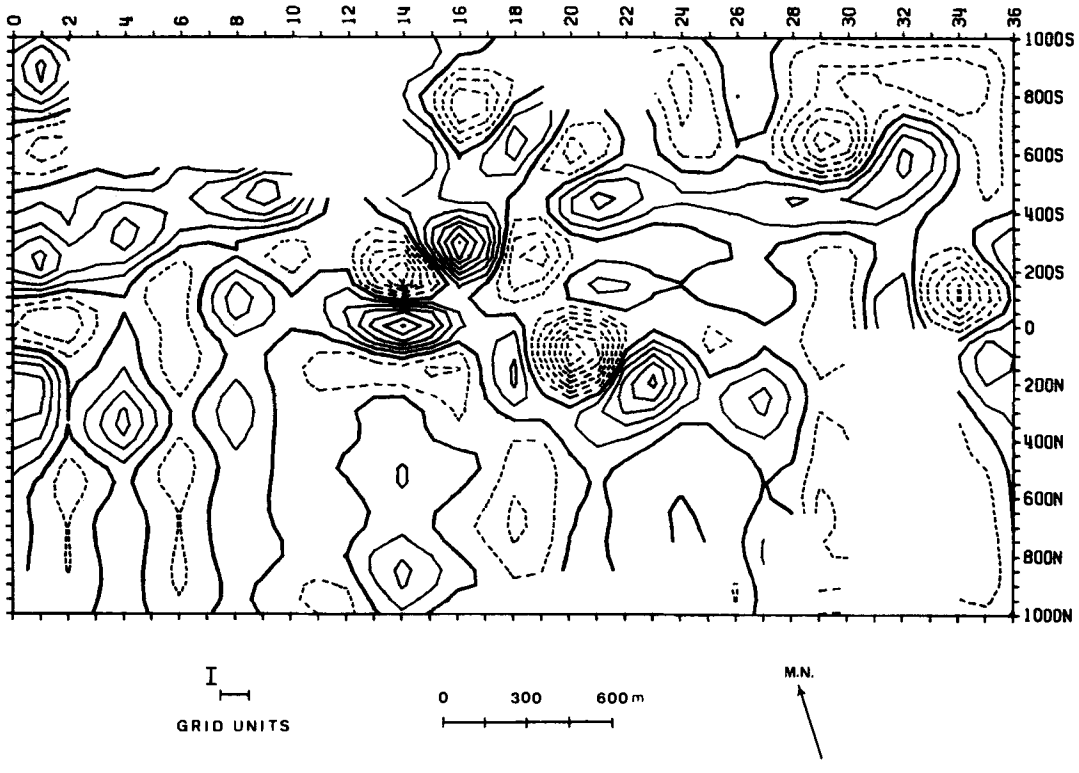

FIG. 10. Magnetization map computed with $\lambda = 0.5$ from the reduced-to-the-pole map (not shown) obtained from the total field map of Figure 9. Dashed lines represent negative values and the contour interval is 0.5 A/m.

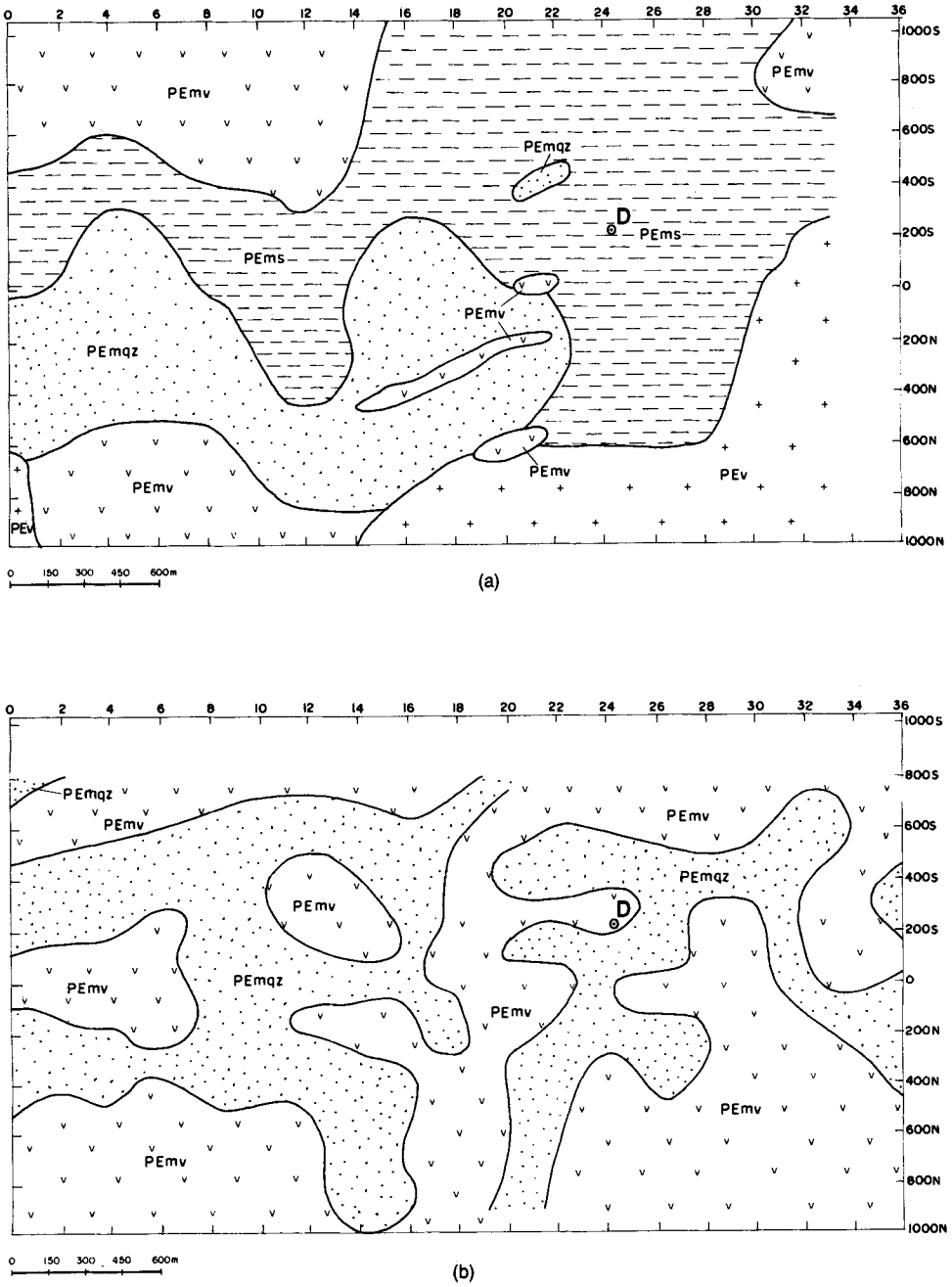

FIG. 11. (a) Preliminary geologic map of the Xingú River Basin area. Mapped units comprise acid volcanic rocks consisting of andesite and rhyolite (PEv), metasedimentary rocks, mainly consisting of quartzite, ferruginous quartzite, itabirite (PEmqz), and schist (PEms), and basic metavolcanic rocks (PEmv). (b) Geologic interpretation of the magnetization map of Figure 10.

CONCLUSIONS

We have presented a method for performing linear transformations of potential field data, based on the equivalent-layer principle, which is particularly well suited to process areas containing large amounts of data. The transformations are carried out in the spatial domain by an operation similar to discrete convolution, so that there is virtually no limit to the number of observations which can be processed. Two particular features distinguish our method from other methods employing equivalent sources to process potential field data. First, the computation of the discrete equivalent layer is formulated as an underdetermined least-squares problem. This procedure allows the use of an equivalent layer extending beyond the data window, which allows interfering sources to be taken into account. At the same time, the memory necessary for the transformation is drastically reduced. Second, the underdetermined least-squares pseudoinverse is premultiplied by the central row of the discrete Green's function matrix in order to obtain the transformed field at the central point of the data window. This procedure minimizes edge effects and reduces the total processing time. Besides these advantages, our method shares the useful property of all equivalent-layer processing methods of being able to produce meaningful processed maps even when the transformation is an unstable one.

One restriction to the application of the proposed method is that the observations must have been previously interpolated on a rectangular grid. Another restriction, common to all methods employing discrete equivalent sources, is that the depth of the equivalent layer must be between two and six times the grid spacing (Dampney, 1969).

The method was applied to synthetic and real anomalies, producing in all cases meaningful transformed fields despite the presence of interfering sources and random noise.

ACKNOWLEDGMENTS

We thank PARANAPANEMA S.A. for permission to publish the magnetic map of Xingú River Basin. Financial support for this research was provided by Financiadora de Estudos e Projetos (FINEP), and Conselho Nacional de Desenvolvimento Científico e Tecnológico (CNPq), Brazil.

REFERENCES

Andrade, C. A. C., and Cunha, F. M. B., 1971, Revisão geológica da bacia paleozóica do Amazonas: Annals from the 25th Mtg., Braz. Geol. Soc., **3**, 93–112.

Bhattacharyya, B. K., 1965, Two-dimensional harmonic analysis as a tool for magnetic interpretation: Geophysics, **30**, 829–857.

Black, D. I., and Scollar, I., 1969, Spatial filtering in the wave-vector domain: Geophysics, **34**, 916–923.

Bott, M. H. P., 1967, Solution of the linear inverse problem in magnetic interpretation with application to oceanic magnetic anomalies: Geophys. J. Roy. Astr. Soc., **13**, 313–323.

Bott, M. H. P., and Ingles, A., 1972, Matrix method for joint interpretation of two-dimensional gravity and magnetic anomalies with application to the Iceland-Faeroe Ridge: Geophys. J. Roy. Astr. Soc., **30**, 55–67.

Dampney, C. N. G., 1969, The equivalent source technique: Geophysics, **34**, 39–53.

Elkins, T. A., 1951, The second derivative method of gravity interpretation: Geophysics, **16**, 29–50.

Emilia, D. A., 1973, Equivalent sources used as an analytic base for processing total magnetic field profiles: Geophysics, **38**, 339–348.

Fuller, B. D., 1967, Two-dimensional frequency analysis and design of grid operators, *in* Hansen, D. A., Heinrichs, W. E., Jr., Holmer, R. C., MacDougall, R. E., Rogers, G. R., Sumner, J. S., and Ward, S. H., Eds., Mining geophysics, **II** Theory: Soc. Explor. Geophys., 658–708.

Gunn, P. J., 1975, Linear transformations of gravity and magnetic fields: Geophys. Prosp., **23**, 300–312.

Henderson, R. G., 1960, A comprehensive system of automatic computation in magnetic and gravity interpretation: Geophysics, **25**, 569–585.

Henderson, R. G., and Zietz, I., 1949, The computation of second vertical derivatives of geomagnetic fields: Geophysics, **14**, 508–516.

Hoerl, A. E., and Kennard, R. W., 1970a, Ridge regression: biased estimation for nonorthogonal problems: Technometrics, **12**, 55–67.

——— 1970b, Ridge regression: applications to nonorthogonal problems: Technometrics, **12**, 69–82.

Jupp, D. L. B., and Vozoff, K., 1975, Stable iterative methods for the inversion of geophysical data: Geophys. J. Roy. Astr. Soc., **42**, 957–976.

Kanasewich, E. R., and Agarwal, R. G., 1970, Analysis of combined gravity and magnetic fields in wavenumber domain: J. Geophys. Res., **75**, 5702–5712.

Langel, R. A., Slud, E. V., and Smith, P. J., 1984, Reduction of satellite magnetic anomaly data: J. Geophys., **54**, 207–212.

Linsser, H., 1974, Interpretação de anomalias gravimétricas regionais na área amazônica: Boletim técnico da Petrobrás, **17**, 3–15.

Mayhew, M. A., 1979, Inversion of satellite anomaly data: J. Geophys., **45**, 119–128.

Mayhew, M. A., Johansen, B. D., and Langel, R. A., 1980, An equivalent source model of the satellite-altitude magnetic anomaly field over Australia: Earth Plan. Sci. Lett., **51**, 189–198.

Paine, J. W., 1986, A comparison of methods for approximating the vertical gradient of one-dimensional magnetic field data: Geophysics, **51**, 1725–1735.

Pearson, W. C., and Skinner, C. M., 1982, Reduction-to-the-pole of low-latitude magnetic anomalies: 52nd Ann. Internat. Mtg., Soc. Explor. Geophys., Expanded Abstracts, 356–358.

Penrose, R., 1955, A generalized inverse for matrices: Proc. Cambridge Phil. Soc., **51**, 406–413.

Peters, L. J., 1949, The direct approach to magnetic interpretation and its practical application: Geophysics, **14**, 290–319.

Rao, C. R., and Mitra, S. K., 1971, Generalized inverse of matrices and its applications: John Wiley and Sons, Inc.

Ridgway, J. R., and Hinze, W. J., 1986, MAGSAT scalar anomaly map of South America: Geophysics, **51**, 1472–1479.

Rosenbach, O., 1953, A contribution to the computation of the "second derivative" from gravity data: Geophysics, **18**, 894–909.

Roy, A., 1966, The method of continuation in mining geophysical interpretation: Geoexplor., **4**, 65–83.

Silva, J. B. C., 1986, Reduction to the pole as an inverse problem and its application to low-latitude anomalies: Geophysics, **51**, 369–382.

Silva, J. B. C., and Hohmann, G. W., 1984, Airborne magnetic susceptibility mapping: Explor. Geophys., **15**, 1–13.

Tsay, L. J., 1975, The use of Fourier series method in upward continuation with new improvements: Geophys. Prosp., **23**, 28–41.

von Frese, R. R. B., Hinze, W. J., and Braile, L. W., 1981, Spherical earth gravity and magnetic anomaly analysis by equivalent point source inversion: Earth Plan. Sci. Lett., **53**, 69–83.

——— 1982, Regional North American gravity and magnetic anomaly correlations: Geophys. J. Roy. Astr. Soc., **69**, 745–761.

von Frese, R. R. B., Ravat, D. N., Hinze, W. J., and McGue, C. A., 1988, Improved inversion of geopotential field anomalies for lithospheric investigations: Geophysics, **53**, 375–385.